

Submitted to Ocean Dynamics

08 Jan 2004

**On the sensitivity of the West Caribbean Sea circulation to tides, wind and
mesoscale ocean eddies: A three-dimensional ocean model study**

Thattai, D. V.¹, Ezer, T.², and Kjerfve, B.^{1,3,*}

¹Department of Geological Sciences, University of South Carolina, Columbia, SC 29208

²Atmospheric and Ocean Sciences, Princeton University, Princeton, NJ

³Marine Science Program, University of South Carolina, Columbia, SC 29208

*Corresponding Author. E-mail: bjorn@msci.sc.edu; Phone: 803 777 2572; Fax: 803 777

4600

Abstract

A three-dimensional, primitive equation ocean model is used to study the circulation in the West Caribbean Sea (WCS) region, and to test the sensitivity of the coastal flow to various forcing fields such as tides, climatological wind, and Caribbean eddies. The model domain is bordered by latitudes $15 - 22^\circ$ N and longitudes $76 - 87^\circ$ W, with the MesoAmerican Barrier Reef System (MBRS, along the coasts of Mexico, Belize, Guatemala, and Honduras) and the southern coast of Cuba as land boundaries. The WCS is open to the Caribbean Sea in the southeast and the Yucatan Channel in the northwest, with a prescribed 25 Sv flow-through from southeast to northwest. The results show that the base flow is highly variable even without time dependent forcing and without assimilation of eddies. The interaction of the base flow with the bathymetry gives rise to frequent westward propagating cyclonic eddies with diameters of 50-150 km in the Gulf of Honduras, and an anticyclonic eddy southeast of the Yucatan Channel with diameter of 200 km. When mesoscale eddies are included in the initial condition through assimilation of altimeter data, the WCS model simulates the propagation of those eddies, so that the eddy field is quite realistic even after 45 days from the initialization. Moreover, eddies were found to influence the coastal flow, such that when a cyclonic or an anticyclonic eddy is propagating through the WCS, the velocity field along the MBRS is either attenuated or enhanced, respectively. The area-averaged mean surface kinetic energy is influenced mostly by the 25 Sv flow-through and climatological winds, while the area-averaged eddy surface kinetic energy is influenced mostly by the mesoscale Caribbean eddies.

Keywords: MesoAmerican Reef, Caribbean Sea, Princeton Ocean Model, eddies, numerical model

1 Introduction

Advances in the understanding of ocean physics and improvements in computational technology and resources have led to the development of various complex numerical 3D ocean models (McWilliams 1998). These models can provide useful tools to study important processes relevant to the ecologically sensitive coastal West Caribbean Sea region such as land-runoff, and transport of pollutants, larvae, and nutrients. However, one of the most difficult challenges in ocean modeling is to couple the large-scale ocean circulation with near-shore coastal processes, as it involves large range of dynamical scales and sharp topographic changes. The oceanic circulation of the open ocean and its variability are however important factors influencing the coastal circulation and to understand coastal flow variability requires an understanding of open ocean dynamics as well.

The West Caribbean Sea (WCS) is defined here as the portion of the Caribbean Sea bounded between $15 - 22^{\circ}$ N and $76 - 87^{\circ}$ W (Fig. 1). The MesoAmerican Barrier Reef, along of the coasts of Mexico, Belize, Guatemala, and Honduras, forms the western boundary and the Caribbean coast of Cuba forms the eastern boundary. The WCS is open to the Caribbean Sea in the southeast and to the Gulf of Mexico through the Yucatan Channel in the northwest. The Cayman Basin which lies between the Nicaragua Rise and the Cayman Ridge has depths of more than 5000 m, and waters as deep as 2000 m cut into the Gulf of Honduras within 15 km from the MesoAmerican Barrier Reef. The MesoAmerican Barrier Reef System (MBRS) extends for more than 1000 km from Isla

Contoy at the northern corner of the Yucatan (Mexico) to the Bay Islands (Honduras) (Fig. 1) (Almada-Villela et al. 2003). The Yucatan Basin lies between the Cayman Ridge and the Yucatan Channel. The variable bathymetry is an important factor in the modification of the eddies that pass through the WCS (Molinari et al. 1981; Sou et al. 1996).

In earlier studies, the Caribbean current was often described as a steady westward flow from the Lesser Antilles through three major deep-water basins and via the Yucatan Channel into the Gulf of Mexico, with little or no variability in the western portion of the Caribbean Sea (Gordon 1967; Brucks 1971). Later studies indicated the presence of some variability in the western Caribbean but even these did not describe in much detail the western Caribbean as they focused on the Caribbean Sea in its entirety (Molinari et al. 1981; Kinder et al. 1985; Carton and Chao, 1999; Andrade and Barton 2000). Sou et al. (1996) applied a numerical model to the Caribbean and simulated the presence of gyres near the Gulf of Honduras (GoH), but only at depths of more than 200 m and not at the surface. Murphy et al. (1999) in their model study focused on the eddy connectivity in the Intra-America Seas. They simulated the formation of mesoscale eddies in the Lesser Antilles and tracked the translation of the eddies in the Caribbean Sea and through the Yucatan Channel. Their model showed greater detail in the Lesser Antilles region but not in the Gulf of Honduras. The minimum depth in the model was 200 m, which entirely excludes the continental shelves. Ezer et al. (2003) and Oey et al. (2003) used more realistic topography near the coast to study the influence of Caribbean eddies and wind

on the variability of the flow in the Yucatan Channel, but did not investigate the influence of the eddies on the western Caribbean Sea itself.

The variability in the WCS is thus still largely an unexplored topic. With limited oceanographic observations of the eddy variability in this region, numerical models can provide more detailed information about the circulation and its variability. Therefore, the Princeton Ocean Model (POM) (Blumberg and Mellor 1987) was adapted and implemented in this region to explore the influence of climatological winds, eddies, and tides on the general circulation and the coastal flows. The changes in variability caused by the different forcing functions are analyzed, in particular for the surface waters. We concentrate in particular on the Gulf of Honduras and the waters bordering the MBRS, which is an ecologically and economically important region in Central America. The advantage of using a sigma vertical grid (terrain-following coordinates) is that it is suitable for applications in the deep ocean as well as on the coastal shelves. This study focuses on the basic sensitivity of the model to different forcings, and is the first step toward more realistic simulations and forecasts, which will be the focus of future research now underway.

2 Model description and setup

The WCS model is based on POM which is a 3D, free surface, primitive equation, finite difference model (Blumberg and Mellor 1987; Mellor 1996). It is a sigma coordinate (terrain-following) model, meaning that the water column is divided into an

equal number of proportional vertical layers regardless of the local depth. Curvilinear orthogonal coordinates define the horizontal grid, and a staggered "Arakawa C" differencing scheme is used for the grid. An explicit time step is used for the horizontal differencing and an implicit scheme for the vertical differencing, which enables the use of fine vertical resolution in the surface and shallow layers. The model employs a split time step. The external mode is two-dimensional and uses a short time step based on the Courant-Friedrich-Lewy (CFL) condition and the external wave speed. The internal mode is three-dimensional and uses a long time step based on the CFL condition and the internal wave speed. The model contains an imbedded second moment turbulence closure scheme to provide vertical mixing coefficients (Mellor and Yamada, 1982).

The transformation of the coordinates to the sigma coordinates is accomplished through

$$x^* = x; y^* = y; \sigma = (z - \eta)/D; t^* = t \quad (1)$$

where x , y , and z are the Cartesian coordinates; $D = H + \eta$ where $H(x, y)$ is the bottom topography and $\eta(x, y, t)$ is the surface elevation. σ varies from $\sigma = 0$ at $z = \eta$ to $\sigma = -1$ at $z = -H$. The governing equations are the continuity equation, the momentum equations, the temperature and salinity equations, the turbulence closure equations, and the equation of state (Mellor and Yamada 1982; Blumberg and Mellor 1987; Mellor 1996), and are listed in Appendix A.

The horizontal mixing coefficient for diffusion is given by a Smagorinsky-type formulation (Smagorinsky et al. 1965) as

$$A_M = C\Delta x\Delta y[(\partial u/\partial x)^2 + (\partial v/\partial x + \partial u/\partial y)^2/2 + (\partial v/\partial y)^2]^{1/2} \quad (2)$$

(see Ezer and Mellor 2000, for model sensitivity studies to this formulation). A_M is proportional to the grid size and to the velocity gradients. The Smagorinsky coefficient C has a value of 0.2 here. The climatological values of T and S , T_{CLIM} and S_{CLIM} , are subtracted from the temperature and salinity in the diffusion terms which reduces the unwanted diapycnal mixing over steep topography (Ezer and Mellor 2000). The General Digital Environmental Model (GDEM) monthly climatology is used for T_{CLIM} and S_{CLIM} , as well as for initialization (Teague et al. 1990).

The domain of the model encompasses the WCS as defined earlier. The grid consists of 20,301 cells with 16 vertical layers. The proportional sigma vertical layers were selected at 0, -0.002, -0.003, -0.007, -0.014, -0.028, -0.056, -0.111, -0.222, -0.333, -0.444, -0.556, -0.667, -0.778, -0.889, and -1.000 of the total local depth. Thus, since temperature, salinity, density, and currents vary most near the surface, the emphasis was on resolving well the variability near the surface. The horizontal grid resolution varies from 3 km along the MBRS to 8 km on the open eastern boundary (Fig. 2), and the depth ranges from 1 m to 6000 m. The bathymetry was interpolated from a $1/24^\circ$ Digital Terrain Model (DTM) grid into the model grid. However, it was necessary to manually correct the model topography along the coastlines using more detailed charts (Fig. 3). Sharp changes in the bathymetry were slightly smoothed following Mellor et al. (1994; 1998). This, and subtraction of the mean vertical profiles, reduce the pressure gradient errors (Mellor et al. 1994; 1998; Ezer et al. 2002). Since our focus here is mainly on the near surface and coastal flows, potential small numerical errors near the deep slopes may

not affect the results. The external time step is 6 s and the internal time step is 3 min. Monthly temperature and wind data were obtained from the Comprehensive Ocean-Atmosphere Data Set (COADS) (<http://www.ncdc.noaa.gov/oa/climate/coads/>), and salinity was interpolated from GDEM (<http://128.160.23.42/gdemv/gdemv.html>). Satellite altimeter data were obtained from the Archiving, Validation, and Interpretation of Satellites Oceanographic (AVISO) data set which combines the TOPEX-Poseidon (T/P) and ERS satellite altimeter measurements (Ducet et al. 2000).

The open ocean boundary conditions for the inflow and outflow barotropic transports are interpolated from a coarser-scale North Atlantic POM (Ezer and Mellor 2000). The flow boundary condition is a radiation condition on the v-velocity in the north and south. The tangential velocities are set to zero. This is in addition to a 25 Sv throughflow at the southeastern (inflow) and northwestern (outflow) boundaries, distributed along the open boundaries following Ezer and Mellor (2000). Surface heat and salinity fluxes are neglected in this study of relatively short-term simulations. Tidal amplitudes and phases of six constituents (M2, S2, N2, O1, K1, and P1) for the two boundaries were included from data based on Ray's (1999) model and modified according to Kjerfve (1981). The tidal forcing was applied through the barotropic velocity and elevation boundary conditions and body force. The amplitudes and phases on the open boundaries were empirically adjusted to minimize the difference between the model water level and observed water level data from Puerto Cortes (Honduras) and Puerto Morelos (Mexico). Such a practice is common in coastal models (Chen and Mellor 1999; Wong et al. 2003) since the global tidal model is not very accurate in shallow

regions. Fig. 4 shows an example of the observed and modeled water levels at Gladden Spit for the time period 21 Apr – 11 May 1998.

Sea surface height (SSH) anomalies derived from the satellite altimeter data every 10 days are used to introduce eddies into the model, following previous assimilation methodology (Mellor and Ezer 1991; Ezer and Mellor 1994; 1997; Wang et al. 2003). The SSH anomalies are mapped baroclinically into a modified vertical temperature distribution between the surface and 1000 m, assuming that

$$\delta T(x, y, z, t) = F_T(x, y, z) \delta \eta(x, y, t) \quad (3)$$

where F_T is a correlation factor, and $\delta \eta$ is the SSH anomaly. The correlation factor is defined by

$$F_T = \langle \delta T \delta \eta \rangle / (\delta \eta)^2 \quad (4)$$

T_o is the temperature inferred from satellite sea level anomaly, as

$$T_o(x, y, z) = T_{CLIM}(x, y, z) + F_T \delta \eta(x, y) \quad (5)$$

In the data assimilation studies mentioned above, F_T was calculated either from model or data statistics of the surface-to-subsurface correlation, and was a function of location and depth ($F=F(x, y, z)$). In this study, the scheme was simplified and $F=F(z)=A+Bz$ was empirically chosen by adjusting the values of A and B until the model elevation reproduced the observed sea level when initialized with temperature field given in (5). The maximum value of F_T was 0.6 near the surface and zero below 1000m depth. No further assimilation of SSH was done beyond applying the SSH field as a model initial condition.

3 Results and discussion

The flow variability in the western Caribbean has implications for the transport of larvae, nutrients, pollutants, and genetic material over distances corresponding to a variety of length scales. The availability of satellite altimetry data makes it possible to include the sea level anomalies as initial conditions in the model executions, and thus simulate the effect of the mesoscale eddies that enter the WCS domain. The satellite data are effective in resolving mesoscale eddies in the deep basins but are not effective over the shelves. Thus, even though they are assimilated into the model for simulating the effects of the eddies, smaller eddies have to be resolved by the physics of the model (Wang et al. 2003). The predominant eddy movement in the Caribbean Sea includes the propagation of anticyclonic eddies, with length scales of 300-500 km, in the northern half of the region and cyclonic eddies, with length scales of 50-150 km, which irregularly propagate westward along the southern boundary.

Eight different simulations were executed, each of 45 days duration, and the results from the last 30 days of each simulation were used to assess the influence of different forcing functions on the circulation and water level variability in the WCS (Table 1). The mean elevation, mean and eddy kinetic energies, and RMS of currents and elevations for the 30 days were calculated for each simulation, along with mean and RMS differences between the simulations.

Seven simulations were executed for the time period 06 April - 20 May 1998, for which all the data (tides, winds, and eddies) were available. An additional simulation was executed for the time period 29 April – 12 June 1999, when a new set of SSH anomalies was available. The amplitudes and phases of the tide at six stations (Fig. 1, A-F) were compared with observed amplitudes and phases to verify that the model simulates the tidal water level variations reasonably (Table 2). The modeled amplitudes match the observed amplitudes well but there are some discrepancies in the phases. However, the average absolute difference in amplitude for all stations is only 0.5 cm and the average absolute difference in phase is less than 10° overall.

The modeled temperature and salinity profiles seaward of Gladden Spit were compared with CTD profiles to check if the model captures the temperature and salinity profiles. Both the modeled (Simulation #6) and observed profiles correspond to the month of May, and the range of values and the shape of the profiles match closely (Figs. 5a, b).

3.1 General circulation

The general circulation in the WCS in the presence of the 25 Sv flow-through as the only forcing (case #1) consists of a mean flow that enters the southeastern channels and exits the WCS via the Yucatan Channel. This flow is however neither steady nor uniform. The highest velocities occur along the MBRS and the coast of Honduras, with values reaching more than 0.50 m s^{-1} along the northern coast of the Yucatan Peninsula.

As many as five cyclonic gyres appear between the Nicaraguan rise and south of Chinchorro Atoll, along the coast, with the most prominent gyres appearing on the Nicaraguan rise and in the Gulf of Honduras. These gyres have diameters of 50-150 km. There is no clear propagation pattern of these gyres, however, over the time span of 30 days. An anticyclonic eddy of 300 km diameter is also present southeast of the Yucatan Channel, and this eddy traveled 200 km in about 20 days (or a speed of 0.12 m s^{-1}), exiting the model domain through the Yucatan Channel.

The base flow depresses the 30-day mean water level along the MBRS coast from Honduras to the northern tip of the Yucatan Peninsula by as much as 10 cm, and also increases the mean water level along the coast of Cuba by approximately 7-8 cm (Fig. 6a). In general, mesoscale anticyclonic gyres are the continuation, or offshoots, of the eddies formed in the Caribbean Sea south of the Nicaraguan Rise (Murphy et al. 1999), the presence of the cyclonic gyres along the southern coastline is the result of the bathymetric effects on the base flow-through. This suggests that the base flow in the WCS exhibits considerable variability (Fig. 6c), although the variability is less than when winds, tides, and eddies are applied (case #7, Fig. 6d). Addition of climatological winds does not result in a significant change in the mean water levels, but increases the velocities northeast of the GoH to 0.50 m s^{-1} . The velocities southwest of the Yucatan Channel are as high as 0.75 m s^{-1} . The mean elevation for Simulation #7 (Fig. 6b) shows an increase of 3-4 cm over the base case in the Yucatan Basin.

The strengthening or weakening of cyclonic gyres in the inner GoH is influenced by the frequency and strength of the cyclonic and anticyclonic eddies passing through the WCS. The simulation in case #3 involved initialization of the model with altimeter data corresponding to the SSH anomaly field for 04 Apr 1998. The 30-day circulation plots corresponding to this simulation show the presence of cyclonic gyres along the coast of Honduras and also south of Chinchorro Atoll, each with a diameter on the order of 50 - 150 km. There also exists a weak cyclonic gyre that passes north of GoH at the same time. The addition of climatological winds (Simulation #7) intensified energetics in the entire system, disintegrated the cyclonic eddy east of the Bay Islands, and increased the size and number of anticyclonic eddies in the WCS in general. In comparison, when the model was initialized with the SSH anomaly field corresponding to 29 Apr 1999 (Simulation #8), there was a strong anticyclonic gyre passing through the WCS that diminished the strength of the cyclonic gyre in the inner GoH in the latter half of the simulation, when the anticyclonic gyre was passing just north of the GoH (Fig. 7).

The SSH anomalies calculated from Simulations #7 and #8 (for the years 1998 and 1999) were compared with the SSH anomalies for the same dates from the satellite data. The model is able to simulate the propagation of the eddies quite well even 45 days after the initial assimilation (Fig 8a, b and Fig. 9a, b). The cyclonic eddy that transited the WCS in Simulation #7 traveled approximately 220 km in 30 days, which means that it could take up to 10-12 months to cross the entire WCS from southeast to northwest. This translates to a travel speed of $\sim 0.09 \text{ m s}^{-1}$. This value is somewhat smaller than the propagation speed reported in the literature for Caribbean eddies (0.12 m s^{-1} , Carton and

Chao 1999; 0.15 m s^{-1} , Murphy et al. 1999). However, the models used are different, and the simulations in this study are of shorter duration and may thus not resolve the long-term eddy transit times well, even though the model bathymetry is much more detailed for the WCS.

3.2 Variability in the Gulf of Honduras and MBRS

The interaction of the base flow with the bathymetry along the MBRS results in high variability along the reefs/coastline. The rms water level elevation is 7-8 cm (Fig. 6c). The variability is reduced in the deeper basins. The presence of high water level variability in the absence of other forcing functions suggests that the flow in the WCS is far from steady, subjected to flow meanders effects caused by interactions with the bathymetry. The addition of winds (case #2) to the base flow greatly reduces the rms variability along the coast, to 2-3 cm, and even more so in the inner GoH and around the Bay Islands. The rms variability along the MBRS coast also reduces when T/P-ERS altimeter data are added as an initial condition in the simulations, but the rms variability northeast of the Bay Islands is increased, corresponding to the presence of the westward-propagating cyclonic gyre. As can be expected, the addition of tides greatly increases the overall variability in the region. Variability is especially high along the coastline from Mexico to Honduras, where the 30-day rms elevation increases by 6-7 cm over the base case. The rms plot for Simulation #7 (Fig. 6d) shows the highest water level variability resulting from the sum cause of all forcing mechanisms, including preexisting eddies as an initial condition.

3.3 Mean and eddy surface kinetic energy (SKE)

The flow through the WCS is not steady and uniform but highly variable. It is useful to look at the kinetic energies as a measure of the variability associated with the flows. A considerable amount of the kinetic energy in the oceans is due to turbulent mesoscale eddies rather than the mean flow (Knauss 1996; Kantha and Clayson 2000). These eddies transport large quantities of water and thus materials, and the rate of transfer of water/materials to the surrounding waters depends on their energy levels. The mean SKE represents the strength of the mean flow and can indicate the relative importance of the forcing functions. The eddy kinetic energy, likewise, represents the importance of the meanders and eddies that are superimposed on the mean circulation.

The area-averaged mean SKE was calculated as

$$\frac{\sum_{j=1}^n 0.5 \Delta x_j \Delta y_j (u_j^2 + v_j^2)}{\sum_{j=1}^n \Delta x_j \Delta y_j} \quad (19)$$

and the eddy SKE was calculated as

$$\frac{\sum_{j=1}^n 0.5 \Delta x_j \Delta y_j ((u_j - \bar{u})^2 + (v_j - \bar{v})^2)}{\sum_{j=1}^n \Delta x_j \Delta y_j} \quad (20)$$

where n is the total number of grids (20,301), and $\bar{u} = \frac{1}{T} \sum_{j=1}^n u_j$. Figures 10a and 10b

represent the 1998 eddies, and Figures 10c and 10d the 1999 eddies, along with cases 1,

2, 4, and 7/8. The plots suggest that the surface mean kinetic energies stabilize in 10 days, thus reinforcing the validity of the model executions for a 45-day period. The area-averaged mean SKE is similar for simulations #1 and #4 (base flow and tides) (Figs. 10a, c, solid and dash-dot lines) which suggests that the tides do not contribute any significant energy to the mean flow in addition to the base case. This is consistent with the harmonic analysis of current meter time series along the MBRS, which showed no significant tidal constituent although the water level harmonics (M_2 , S_2 , N_2 , K_1 , and O_1) were significant at the 95% level. The mean SKE for winds, however, is much larger, with a mean SKE of $0.021 \text{ m}^2 \text{ s}^{-2}$ as compared to $0.013 \text{ m}^2 \text{ s}^{-2}$ for the base case alone (Figs. 10a, c, dashed lines). Thus climatological mean winds explain a significant increase in the SKE. The mean SKE for simulation #7 (diamonds, Fig. 10a), which includes all forcing mechanisms (with 1998 eddies as initial condition), is lower than in the case of simulation #2 (winds), because of the influence of the weak cyclonic eddy centered at 18° N and 85° W that passes westward through the WCS during this time period (Fig. 10a). The mean SKE for eddies corresponding to the 1998 simulation is lower than the base flow and tide cases (Fig. 10a, dotted line), whereas the mean SKE for eddies corresponding to the 1999 simulation increases after 25 days and reaches $0.017 \text{ m}^2 \text{ s}^{-2}$, which is $0.004 \text{ m}^2 \text{ s}^{-2}$ greater than for simulations #1 and #4 (Fig. 10c, dotted line). The mean SKE of $0.023 \text{ m}^2 \text{ s}^{-2}$ for simulation #8 (with 1999 eddies) is higher than that of all the other cases (Fig. 10c). In this simulation, an anticyclonic eddy propagated through the WCS, resulting in an intensification of the velocity field, and thus of the SKEs. In conclusion, the mean SKE exists for the base flow alone, is influenced by both eddies and winds, but tides have little effect. The area-averaged eddy SKE for the 1998 simulation

shows no appreciable effect of the eddies (Fig. 10b) over the other cases (#s 1, 2, and 4) which suggests that the cyclonic eddy that propagated in Apr-May 1998 was weak in nature. However, the eddy SKE for 1999 (simulations #3 and #8) reaches $0.004 \text{ m}^2 \text{ s}^{-2}$ (Fig. 10d), which is twice the value of the eddy SKE for the other simulations (1, 2, and 4). This likewise suggests that anticyclonic eddy that propagated in May-Jun 1999 was of a stronger nature.

3.4 Time series of velocity

Time series plots of u and v velocities for Lighthouse Reef exhibit features representative of the other measurement stations along the seaward edge of the MBRS (Figs. 11a, b). The effect of tides in the current records is not discernable in the velocity time series along the MBRS. The velocities are directed either northeast or northwest at Puerto Cortes, Lighthouse Reef, and Puerto Morelos, but are mainly southeast at Gladden (Fig. 12a, b) and Sapodilla, confirming the presence of a mostly southerly flow along the southern reef between Gladden Spit and the Sapodilla Cays. The effect of the eddies on the north-south v -velocities is shown in Figure 13 (a, b). The cyclonic eddy in 1998 acts against the mean flow and reduces the velocities at Lighthouse Reef (Fig. 13a, dashed line). It also lowers the v -velocity at Gladden Spit (Fig. 13b, dashed line). The anticyclonic eddy in 1999 started to propagate towards the MBRS coast halfway through the simulation execution, and it thus augments the v -velocity (Fig. 13a, dash-dot line). However, the v -velocity is again reduced below the base flow values at Gladden Spit (Fig. 13b, dash-dot line) during this time period. This is because Lighthouse Reef is in the

direct path of the eddies, whereas Gladden Spit is located further away from the zone of influence of the eddies.

4 Conclusions

The three-dimensional Princeton Ocean Model was used to model the circulation in the West Caribbean Sea (WCS). Eight simulations were executed with different forcing functions (wind, tides) and initial conditions (altimetry data). The results show that

- The 25 Sv through-flow (base flow) in the WCS causes large current meanders and eddy variability even in the absence of tides and winds and without forcing by altimetry data to simulate eddy effects as an initial condition. Flow velocities are as high as 0.50 m s^{-1} along the seaward edge of the MesoAmerican Barrier Reef System (MBRS).
- The base flow results in the reduction of sea level along the MBRS coast by 10 cm. The mean flow is characterized by a southeast-northwest flow accompanied by as many as five cyclonic gyres along the Honduran coast in the Gulf of Honduras (GoH), each with diameter 50-150 km, and by the propagation of an anticyclonic eddy with a 300 km diameter southeast of the Yucatan Channel.
- The WCS model is able to simulate well the propagation of mesoscale eddies even 45 days after initialization with altimetry data.
- A typical mesoscale eddy that transits the WCS travels approximately 220 km in 30 days, which means that it could take up to 10-12 months to cross the entire

WCS from southeast to northwest. This translates to a travel speed of $\sim 9 \text{ cm s}^{-1}$, which is slightly slower than previous calculations.

- The area-averaged mean surface kinetic energy is influenced mainly by the through-flow and the climatological winds, while the area-averaged eddy surface kinetic energy is increased when the T/P-ERS eddy field is used as an initial condition. Tides do not show any appreciable increase of the kinetic energies.
- The velocity field along the MesoAmerican Barrier Reef is intensified when there is an anticyclonic mesoscale eddy propagating through the WCS, and attenuated when a cyclonic eddy propagates through the WCS. The number and frequency of cyclonic gyres in the inner GoH and northern coast of Honduras are influenced by the frequency, strength, and nature (cyclonic/anticyclonic) of the mesoscale eddies passing through the WCS, with as many as five cyclonic eddies present in the GoH at times, which reduces to three at other times.

This study was the first step in testing the sensitivity of the WCS model to the basic forcing fields under idealized conditions, so the influence of each element can be evaluated. Future studies now underway will add more realistic features such as high frequency wind variations, surface heat fluxes and extending the domain beyond the barrier reef, so that longer simulations and more detailed direct comparisons with observations will be possible.

Acknowledgments This research was sponsored by funding from the MBRS (MesoAmerican Barrier Reef System) Project and the Nature Conservancy's Ecosystem Research Program/Mellon Foundation. We thank Dr. William D. Heyman and Dra. Patricia Almada-Villela for their help. T.E is partly supported by grants from the Minerals Management Service (MMS) and the Office for Naval Research (ONR).

Appendix A

The 3D governing equations (after dropping the asterisks) may be written as,

$$\frac{\partial DU}{\partial x} + \frac{\partial DV}{\partial y} + \frac{\partial \omega}{\partial \sigma} + \frac{\partial \eta}{\partial t} = 0 \quad (\text{A1})$$

$$\begin{aligned} \frac{\partial UD}{\partial t} + \frac{\partial U^2 D}{\partial x} + \frac{\partial UVD}{\partial y} + \frac{\partial U\omega}{\partial \sigma} - fVD + gD \frac{\partial \eta}{\partial x} \\ + \frac{gD^2}{\rho_o} \int_{\sigma}^{\sigma'} \left[\frac{\partial \rho'}{\partial x} - \frac{\sigma'}{D} \frac{\partial D}{\partial x} \frac{\partial \rho'}{\partial \sigma'} \right] d\sigma' = \frac{\partial}{\partial \sigma} \left[\frac{K_M}{D} \frac{\partial U}{\partial \sigma} \right] + F_x \end{aligned} \quad (\text{A2})$$

$$\begin{aligned} \frac{\partial VD}{\partial t} + \frac{\partial UVD}{\partial x} + \frac{\partial V^2 D}{\partial y} + \frac{\partial V\omega}{\partial \sigma} + fUD + gD \frac{\partial \eta}{\partial y} \\ + \frac{gD^2}{\rho_o} \int_{\sigma}^{\sigma'} \left[\frac{\partial \rho'}{\partial y} - \frac{\sigma'}{D} \frac{\partial D}{\partial y} \frac{\partial \rho'}{\partial \sigma'} \right] d\sigma' = \frac{\partial}{\partial \sigma} \left[\frac{K_M}{D} \frac{\partial V}{\partial \sigma} \right] + F_y \end{aligned} \quad (\text{A3})$$

$$\frac{\partial TD}{\partial t} + \frac{\partial TUD}{\partial x} + \frac{\partial TVD}{\partial y} + \frac{\partial T\omega}{\partial \sigma} = \frac{\partial}{\partial \sigma} \left[\frac{K_H}{D} \frac{\partial T}{\partial \sigma} \right] + F_T - \frac{\partial R}{\partial z} \quad (\text{A4})$$

$$\frac{\partial SD}{\partial t} + \frac{\partial SUD}{\partial x} + \frac{\partial SVD}{\partial y} + \frac{\partial S\omega}{\partial \sigma} = \frac{\partial}{\partial \sigma} \left[\frac{K_H}{D} \frac{\partial S}{\partial \sigma} \right] + F_S \quad (\text{A5})$$

$$\begin{aligned} \frac{\partial q^2 D}{\partial t} + \frac{\partial Uq^2 D}{\partial x} + \frac{\partial Vq^2 D}{\partial y} + \frac{\partial \omega q^2}{\partial \sigma} = \frac{\partial}{\partial \sigma} \left[\frac{K_q}{D} \frac{\partial q^2}{\partial \sigma} \right] \\ + \frac{2K_M}{D} \left[\left(\frac{\partial U}{\partial \sigma} \right)^2 + \left(\frac{\partial V}{\partial \sigma} \right)^2 \right] + \frac{2g}{\rho_o} K_H \frac{\partial \tilde{\rho}}{\partial \sigma} - \frac{2Dq^3}{B_1 \ell} + F_q \end{aligned} \quad (\text{A6})$$

$$\begin{aligned} \frac{\partial q^2 \ell D}{\partial t} + \frac{\partial Uq^2 \ell D}{\partial x} + \frac{\partial Vq^2 \ell D}{\partial y} + \frac{\partial \omega q^2 \ell}{\partial \sigma} = \frac{\partial}{\partial \sigma} \left[\frac{K_q}{D} \frac{\partial q^2 \ell}{\partial \sigma} \right] \\ + E_1 \ell \left(\frac{K_M}{D} \left[\left(\frac{\partial U}{\partial \sigma} \right)^2 + \left(\frac{\partial V}{\partial \sigma} \right)^2 \right] + E_3 \frac{g}{\rho_o} K_H \frac{\partial \tilde{\rho}}{\partial \sigma} \right) \tilde{W} - \frac{Dq^3}{B_1} + F_\ell \end{aligned} \quad (\text{A7})$$

where U, V are horizontal velocities (m s^{-1}); ω is the transformed sigma coordinate vertical velocity (m s^{-1}); f is Coriolis parameter (s^{-1}); g is gravitational acceleration (9.81 m s^{-2}); ρ_0 is reference density (1025 kg m^{-3}); $\rho' = (\rho - 1000) / \rho_0$ is non-dimensional density; K_M is vertical kinematic viscosity ($\text{m}^2 \text{ s}^{-1}$); K_H is vertical diffusivity ($\text{m}^2 \text{ s}^{-1}$); T is potential temperature ($^\circ\text{C}$); R is short wave radiation flux ($\text{m s}^{-1} \text{ K}$); S is salinity (psu); q^2 is twice the turbulence kinetic energy ($\text{m}^2 \text{ s}^{-2}$); l is turbulence length scale (m); $\tilde{W} = 1 + E_2(\ell / kL)$ is the wall-proximity function, where $L^{-1} = (\eta - z)^{-1} + (H - z)^{-1}$, E_2 is a constant (1.33), and k is von Karman constant (0.4); E_1, E_3 are constants; and B_l is a turbulence closure constant. The transformation of ω to the Cartesian vertical velocity is achieved through

$$W = \omega + U \left(\sigma \frac{\partial D}{\partial x} + \frac{\partial \eta}{\partial x} \right) + V \left(\sigma \frac{\partial D}{\partial y} + \frac{\partial \eta}{\partial y} \right) + \sigma \frac{\partial D}{\partial t} + \frac{\partial \eta}{\partial t}$$

The horizontal viscosity and diffusion terms are defined according to

$$F_x \equiv \frac{\partial}{\partial x} (H\tau_{xx}) + \frac{\partial}{\partial y} (H\tau_{xy}) \quad (\text{A8})$$

$$F_y \equiv \frac{\partial}{\partial x} (H\tau_{xy}) + \frac{\partial}{\partial y} (H\tau_{yy}) \quad (\text{A9})$$

where

$$\tau_{xx} = 2A_M \frac{\partial U}{\partial x}, \quad \tau_{xy} = \tau_{yx} = A_M \left(\frac{\partial U}{\partial y} + \frac{\partial V}{\partial x} \right), \quad \tau_{yy} = 2A_M \frac{\partial V}{\partial y} \quad (\text{A10a,b,c})$$

Also,

$$F_\phi \equiv \frac{\partial}{\partial x} (Hq_x) + \frac{\partial}{\partial y} (Hq_y) \quad (\text{A11})$$

where

$$q_x \equiv A_H \frac{\partial \phi}{\partial x}, \quad q_y \equiv A_H \frac{\partial \phi}{\partial y} \quad (\text{A12a,b})$$

ϕ represents T , S , q^2 or $q^2 \ell$; A_M is horizontal kinematic viscosity ($\text{m}^2 \text{s}^{-1}$); and A_H is horizontal heat diffusivity ($\text{m}^2 \text{s}^{-1}$).

The 2D external mode equations are obtained by integrating the internal mode equations over the depth. The equation for the surface elevation is written as

$$\frac{\partial \eta}{\partial t} + \frac{\partial \bar{U}D}{\partial x} + \frac{\partial \bar{V}D}{\partial y} = 0 \quad (\text{A13})$$

The momentum equations are

$$\begin{aligned} \frac{\partial \bar{U}D}{\partial t} + \frac{\partial \bar{U}^2 D}{\partial x} + \frac{\partial \bar{U}\bar{V}D}{\partial y} - \tilde{F}_x - f\bar{V}D + gD \frac{\partial \eta}{\partial x} = -\langle wu(0) \rangle + \langle wu(-1) \rangle \\ + G_x - \frac{gD}{\rho_o} \int_{-1}^0 \int_{\sigma}^0 \left[D \frac{\partial \rho'}{\partial x} - \frac{\partial D}{\partial x} \sigma' \frac{\partial \rho'}{\partial \sigma} \right] d\sigma' d\sigma \end{aligned} \quad (\text{A14})$$

$$\begin{aligned} \frac{\partial \bar{V}D}{\partial t} + \frac{\partial \bar{U}\bar{V}D}{\partial x} + \frac{\partial \bar{V}^2 D}{\partial y} - \tilde{F}_y + f\bar{U}D + gD \frac{\partial \eta}{\partial y} = -\langle wv(0) \rangle + \langle wv(-1) \rangle \\ + G_y - \frac{gD}{\rho_o} \int_{-1}^0 \int_{\sigma}^0 \left[D \frac{\partial \rho'}{\partial y} - \frac{\partial D}{\partial y} \sigma' \frac{\partial \rho'}{\partial \sigma} \right] d\sigma' d\sigma \end{aligned} \quad (\text{A15})$$

The overbars denote vertically integrated velocities such as

$$\bar{U} \equiv \int_{-1}^0 U d\sigma \quad (\text{A16})$$

The wind stress components are $-\langle wu(0) \rangle$ and $-\langle wv(0) \rangle$, and the bottom stress components are $-\langle wu(-1) \rangle$ and $-\langle wv(-1) \rangle$. The quantities \tilde{F}_x and \tilde{F}_y are defined according to

$$\tilde{F}_x = \frac{\partial}{\partial x} \left[H2\bar{A}_M \frac{\partial \bar{U}}{\partial x} \right] + \frac{\partial}{\partial y} \left[H\bar{A}_M \left(\frac{\partial \bar{U}}{\partial y} + \frac{\partial \bar{V}}{\partial x} \right) \right] \quad (\text{A17})$$

$$\text{and } \tilde{F}_y = \frac{\partial}{\partial y} \left[H2\bar{A}_M \frac{\partial \bar{V}}{\partial y} \right] + \frac{\partial}{\partial x} \left[H\bar{A}_M \left(\frac{\partial \bar{U}}{\partial y} + \frac{\partial \bar{V}}{\partial x} \right) \right] \quad (\text{A18})$$

The so-called dispersion terms are defined according to

$$G_x = \frac{\partial \bar{U}^2 D}{\partial x} + \frac{\partial \bar{U} \bar{V} D}{\partial y} - \tilde{F}_x - \frac{\partial \bar{U}^2 D}{\partial x} - \frac{\partial \bar{U} \bar{V} D}{\partial y} + \bar{F}_x \quad (\text{A19})$$

$$G_y = \frac{\partial \bar{U} \bar{V} D}{\partial x} + \frac{\partial \bar{V}^2 D}{\partial y} - \tilde{F}_y - \frac{\partial \bar{U} \bar{V} D}{\partial x} - \frac{\partial \bar{V}^2 D}{\partial y} + \bar{F}_y \quad (\text{A20})$$

References

Almada-Villela PC, Sale PF, Gold-Bouchot B, Kjerfve B (2003) *MBRS Technical Document No. 4*. MBRS Project, Belize, Guatemala, Honduras and Mexico. Belize City, 146 pp

Andrade CA, Barton ED (2000) Eddy development and motion in the Caribbean Sea. *Journal of Geophysical Research*, 105(C11): 26,191-26,201

Blumberg AF, Mellor GL (1987) A description of a three-dimensional coastal ocean circulation model. In: Heaps NS (Ed.) *Three-Dimensional Coastal Ocean Models*, vol. 4, American Geophysical Union, Washington, DC, pp.1-16

Brucks JT (1971) Currents of the Caribbean and adjacent regions as deduced from drifter studies. *Bulletin of Marine Science*, 21(2): 455-465

Carton JA, Chao (1999) Caribbean Sea eddies inferred from TOPEX/POSEIDON altimetry and a $1/6^\circ$ Atlantic Ocean model simulation. *Journal of Geophysical Research*, 104(C4): 7743-7752

Chen P, Mellor GL (1999) Determination of tidal boundary forcing using tide station data. In: Mooers CNK (Ed.) *Coastal Ocean Prediction, Coastal and Estuarine Studies*, 56, American Geophysical Union, Washington, DC, pp. 329-351

Ducet N, Le Tron PY, Reverdin G (2000) Global high-resolution mapping of ocean circulation from TOPEX/Poseidon and ERS-1 and -2. *Journal of Geophysical Research*, 105: 19,477-19,498

Ezer T, Mellor GL (1994) Continuous assimilation of Geosat altimeter data into a three-dimensional primitive equation Gulf Stream model. *Journal of Physical Oceanography*, 24: 832-847

Ezer T, Mellor GL (1997) Data assimilation experiments in the Gulf Stream region: How useful are satellite-derived surface data for nowcasting the subsurface fields?. *Journal of Atmospheric and Oceanic Technology*, 16(6): 1379-1391

Ezer T, Mellor GL (2000) Sensitivity studies with the North Atlantic sigma coordinate Princeton Ocean Model. *Dynamics of Atmospheres and Oceans*, 32: 185-208

Ezer T, Arango H, Shchepetkin AF (2002) Developments in terrain-following ocean models: intercomparisons of numerical aspects. *Ocean Modelling*, 4: 249-267

Ezer T, Oey L.-Y, Lee H.-C, Sturges W (2003) The variability of currents in the Yucatan Channel: Analysis of results from a numerical ocean model. *Journal of Geophysical Research*, 108(C1): 3012, doi: 10.1029/2002JC001509

Gordon AL (1967) Circulation of the Caribbean Sea. *Journal of Geophysical Research*, 72(24): 6207-6223

Kantha LH, Clayson CA (2000) *Numerical Models of Oceans and Oceanic Processes*, International Geophysics Series vol. 66, Academic Press, 940 pp

Kjerfve B (1981) Tides of the Caribbean Sea. *Journal of Geophysical Research*, 86(C5): 4243-4247

Kinder TH (1983) Shallow currents in the Caribbean Sea and Gulf of Mexico as observed with satellite-tracked drifters. *Bulletin of Marine Science*. 33: 239-246

Knauss JA (1996) *Introduction to Physical Oceanography*. Prentice Hall Inc., NJ, 309 pp

McWilliams JC (1998) Oceanic General Circulation Models. In: Chassignet EP, Verron J (Eds.) *Ocean Modeling and Parameterization*, Kluwer Academic Publishers, pp. 1-44

Mellor GL (1996) Users guide for a three-dimensional, primitive equation, numerical ocean model (June 1996 version), *Progress in Atmospheric and Oceanic Sciences*, Princeton University, 38 pp

Mellor GL, Ezer T (1991) A Gulf Stream model and an altimetry assimilation scheme. *Journal of Geophysical Research*, 96, 8779-8795

Mellor GL, Ezer T, Oey L.-Y (1994) The pressure gradient conundrum of sigma coordinate ocean models. *Journal of Atmospheric and Oceanic Technology*, 11: 1126-1134

Mellor GL, Oey L.-Y, Ezer T (1998) Sigma coordinate pressure gradient errors and the seamount problem. *Journal of Atmospheric and Oceanic Technology*, 15(5): 1122-1131

Mellor GL, Yamada T (1982) Development of a turbulent closure model for geophysical fluid problems. *Reviews in Geophysics*, 20: 851-875

Molinari RL, Spillane M, Brooks I, Atwood D, Duckett D (1981) Surface currents in the Caribbean Sea as deduced from Lagrangian observations. *Journal of Geophysical Research*, 86(C7): 6537-6542

Murphy SJ, Hulbert HE, O'Brien JJ (1999) The connectivity of eddy variability in the Caribbean Sea, the Gulf of Mexico, and the Atlantic Ocean. *Journal of Geophysical Research*, 104: 1431-1453

Oey L.-Y, Lee H-C, Schmitz Jr. WJ (2003) Effects of winds and Caribbean eddies on the frequency of loop current eddy shedding: A numerical model study. *Journal of Geophysical Research*, 108(C10): DOI 10.1029/2002JC001698

Ray R (1999) A global ocean tide model from Topex/Poseidon altimetry: GOT99.2, NASA Tech Memo 209478, 58 pp

Smagorinsky J, Manabe S, Holloway JL (1965) Numerical results from a nine-level general circulation model of the atmosphere. *Monthly Weather Review*, 93: 727-268

Sou T, Holloway G, Eby M (1996) Effects of topographic stress on Caribbean Sea circulation. *Journal of Geophysical Research*, 101(C7): 16,449-16,453

Teague WJ, Carron MJ, Hogan PJ (1990) A comparison between the Generalized Digital Environmental Model and Levitus climatologies. *Journal of Geophysical Research*, 95: 7167-7183

Wang D-P, Oey L-Y, Ezer T, Hamilton P (2003) Near-surface currents in DeSoto Canyon (1997-99): Comparison of current meters, satellite observation, and model simulation. *Journal of Physical Oceanography*, 33: 313-326

Wong LA, Chen JC, Xue H, Dong LX, Su JL, Heinke G (2003) A model study of the circulation in the Pearl River Estuary (PRE) and its adjacent coastal waters: 1. Simulations and comparison with observations. *Journal of Geophysical Research*, 108(C5): 3156 DOI 10.1029/2002JC001451

Table 1. Details of forcing functions and altimeter initial conditions used in the eight simulation cases. The wind field is climatological monthly means from COADS. Simulations 3, 6, and 7 included altimetry data from 1998. Simulation 8 included altimetry data from 1999.

Simulation #	Forcing Function			Initial Condition
	25 Sv flow- through	Winds	Tides	SSH anomalies (eddies)
1	√	---	---	---
2	√	√	---	---
3	√	---	---	√
4	√	---	√	---
5	√	√	√	---
6	√	---	√	√
7	√	√	√	√
8	√	√	√	√

Table 2. Observed harmonics and modeled harmonics from Simulation 4, at six stations along the MBRS.

	Observed harmonics		Modeled harmonics		Difference	
	H (cm)	Epoch (G)	H (cm)	Epoch (G)	H (cm)	Epoch (G)
Puerto Morelos (20° 52' N and 86° 52' W) (Station F)						
O1	2.4	347	2.2	333	0.2	14
K1	0.5	254	2.9	268	-2.4	-14
N2	2.5	27	2.1	70	0.4	-43
M2	7.1	52	6.6	52	0.6	0
S2	2.6	44	2.4	24	0.2	20
Lighthouse (17° 26' N and 87° 26' W) (Station E)						
O1	2.2	346	2.3	334	-0.1	13
K1	1.9	268	2.8	267	-0.9	1
N2	2.2	67	2.2	70	0	-3
M2	6.5	84	6.8	82	-0.3	2
S2	2.8	50	2.2	27	0.6	23
Belize City (17° 28' N and 88° 12' W) (Station D)						
O1	3.2	332	2.4	333	0.8	-1
K1	2.3	279	2.8	268	-0.5	11
N2	3.5	76	2.2	70	1.3	6
M2	8.0	84	6.8	82	1.2	2
S2	3.2	36	2.3	27	0.9	9
Gladden (16° 32' N and 87° 59' W) (Station C)						
O1	2.4	331	2.3	334	0.1	-3
K1	2.7	281	2.9	269	-0.2	12
N2	2.3	61	2.2	71	0.1	-10
M2	5.8	87	7.1	91	-1.3	-4
S2	3.0	49	2.3	29	0.7	20
Sapodilla (16° 9' N and 89° 14' W) (Station B)						
O1	2.3	326	2.3	335	0	-9
K1	2.8	262	2.8	268	0	-6
N2	2.4	71	2.2	70	0.2	1
M2	6.1	88	7.2	94	-1.1	-6
S2	2.7	54	2.4	24	0.3	30
Puerto Cortes (15° 50' N and 87° 57' W) (Station A)						
O1	2.5	327	2.3	335	0.2	-8
K1	2.9	269	2.8	268	0.1	1
N2	2.3	71	2.2	71	0.1	0
M2	5.9	86	7.3	98	-1.4	-12
S2	2.3	24	2.2	29	0.1	-5

List of Figures

Figure 1. Model domain of the West Caribbean Sea. A (Puerto Cortes), B (Sapodilla), C (Gladden Spit), D (English Cay), E (Lighthouse Reef), and F (Puerto Morelos) are stations for which some of results are discussed.

Figure 2. Grid used in the West Caribbean Sea model. The model has 20,301 grids, with grid sizes ranging from 3 km – 8 km.

Figure 3. (a) Original bathymetry as interpolated from the Digital Terrain Model. (b) Bathymetry after manual correction along the western boundary.

Figure 4. Observed and modeled water levels at Gladden Spit, Belize for the time period 21 Apr – 11 May 1998.

Figure 5. Observed (dotted line) and modeled (a) temperature and (b) salinity profiles off Gladden Spit during the month of May.

Figure 6. (a) 30-day mean elevations in the WCS for Simulation 1 (base flow). (b) 30-day mean elevations in the WCS for Simulation 7 (all forcing functions with eddy initialization). (c) Root mean square (RMS) of elevations in the WCS for Simulation 1

(base flow). (d) RMS of elevations in the WCS for Simulation 7 (all forcing functions with eddy initialization).

Figure 7. 20-day modeled progression of the 1999 anticyclonic eddy. Each figure is separated by five days. Shown are anomalies of surface elevation and velocity.

Figure 8. (a) Observed and (b) modeled sea surface height and velocity anomalies after 30 days of model execution, Simulation 7.

Figure 9. (a) Observed and (b) modeled sea surface height and velocity anomalies after 30 days of model execution, Simulation 8.

Figure 10. (a) Area-averaged mean surface kinetic energy in the WCS as a function of time. (b) Area-averaged eddy surface kinetic energy in the WCS as a function of time. Solid line: tides; Dash-dot: Base; Dotted line: Eddies (1998); Dashed line: Winds; Diamonds: Base+Tides+Winds+Eddies (1998) for figures a and b. (c) Area-averaged mean surface kinetic energy in the WCS as a function of time. (d) Area-averaged eddy surface kinetic energy in the WCS as a function of time. Solid line: tides; Dash-dot: Base; Dotted line: Eddies (1999); Dashed line: Winds; Diamonds: Base+Tides+Winds+Eddies (1999) for figures c and d.

Figure 11. Velocity vector plots at Lighthouse Reef. (a) T: tides only (Simulation 4); (b) All: tides+winds+eddies (Simulation 7).

Figure 12. Velocity vector plots as Fig. 11, but for Gladden Spit.

Figure 13. (a) v-velocities at Lighthouse Reef for base flow (solid line), 1998 eddy simulation (dashed line), and 1999 eddy simulation (dash-dot line). (b) v-velocities at Gladden Spit for base flow (solid line), 1998 eddy simulation (dashed line), and 1999 eddy simulation (dash-dot line).

Fig. 1

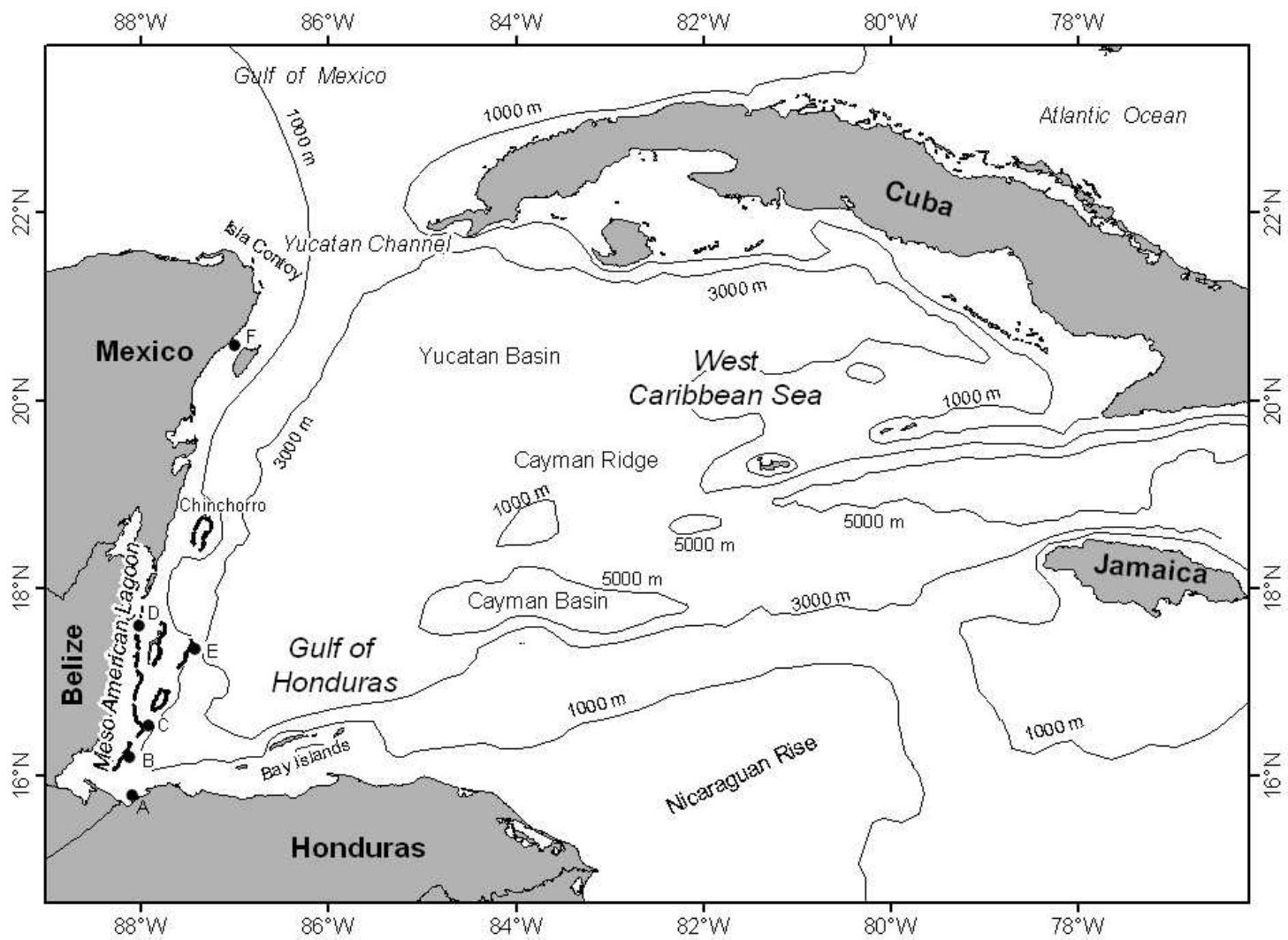


Fig. 2

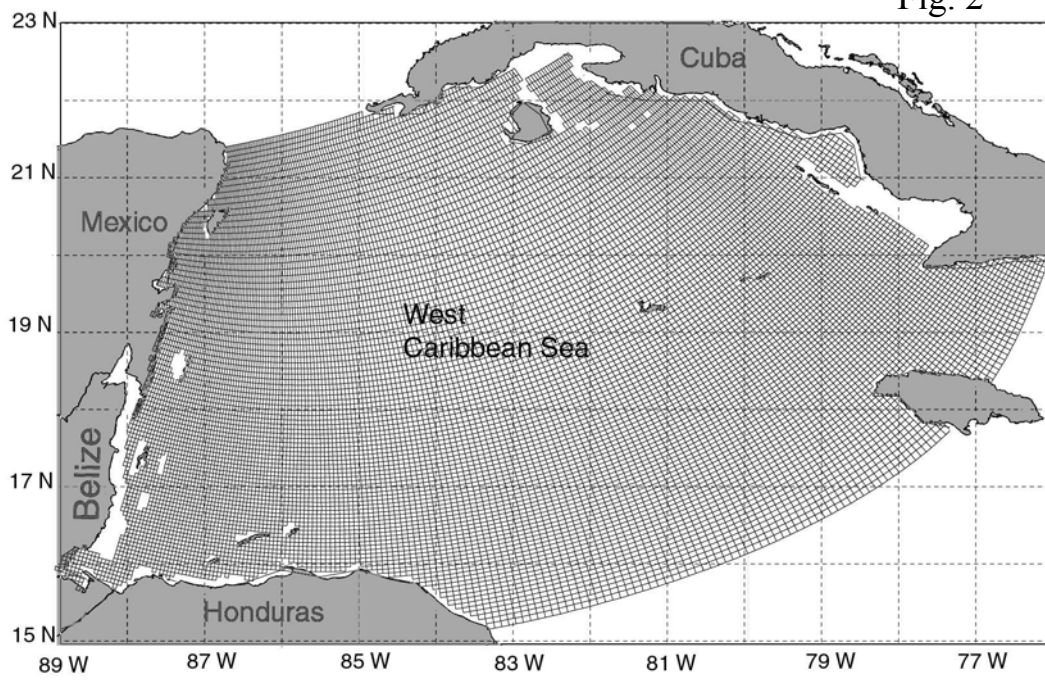


Fig. 3

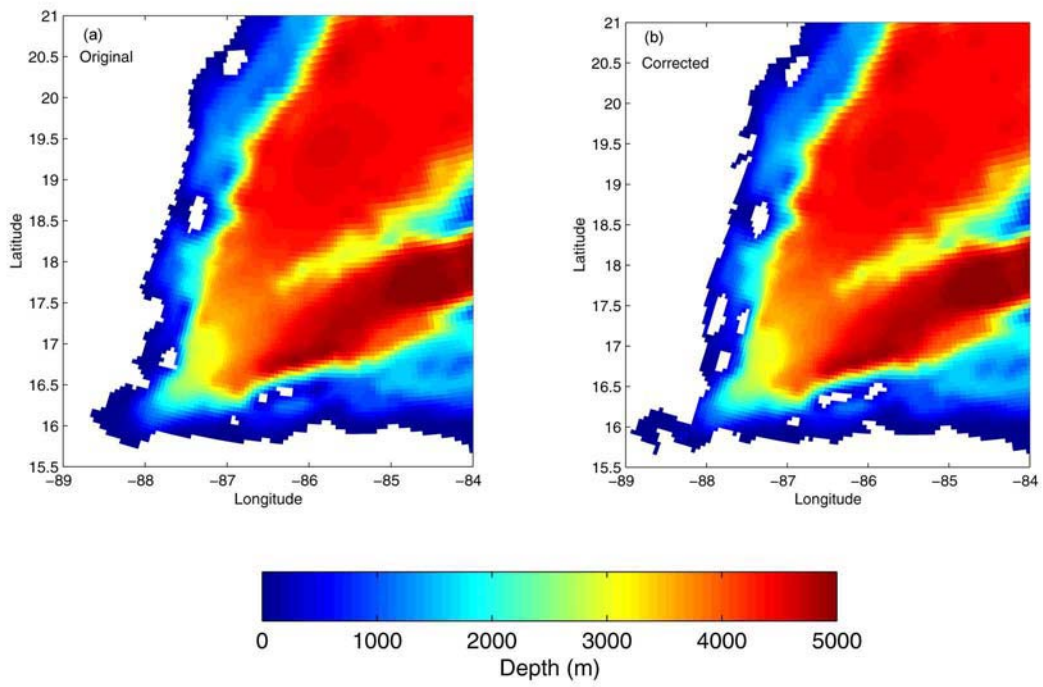


Fig. 4

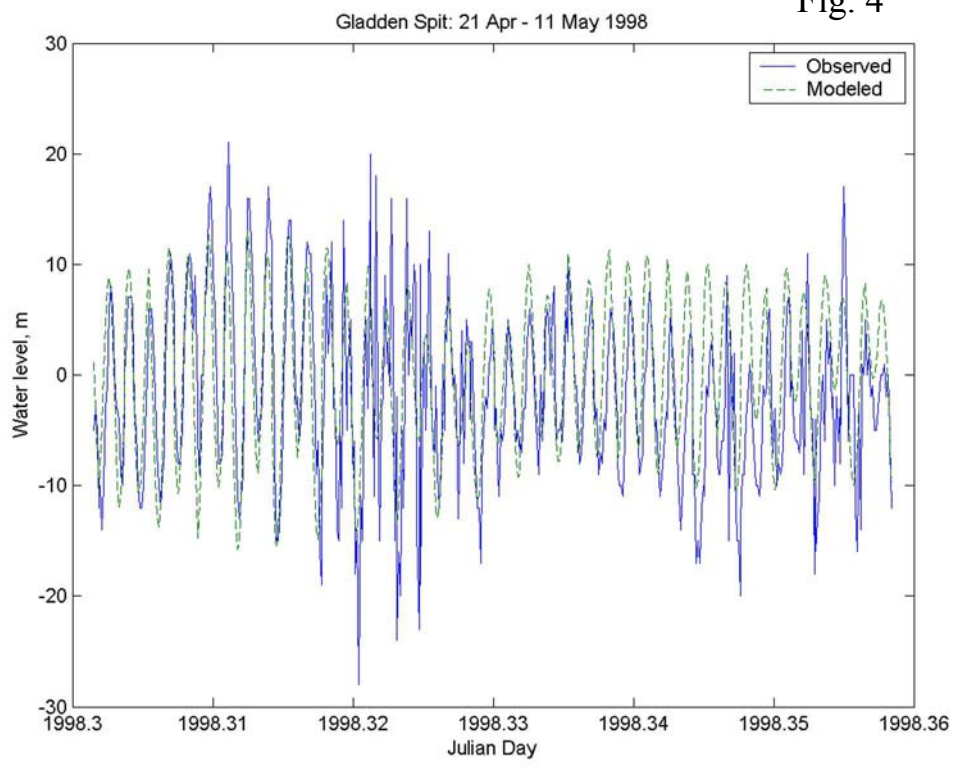


Fig. 5

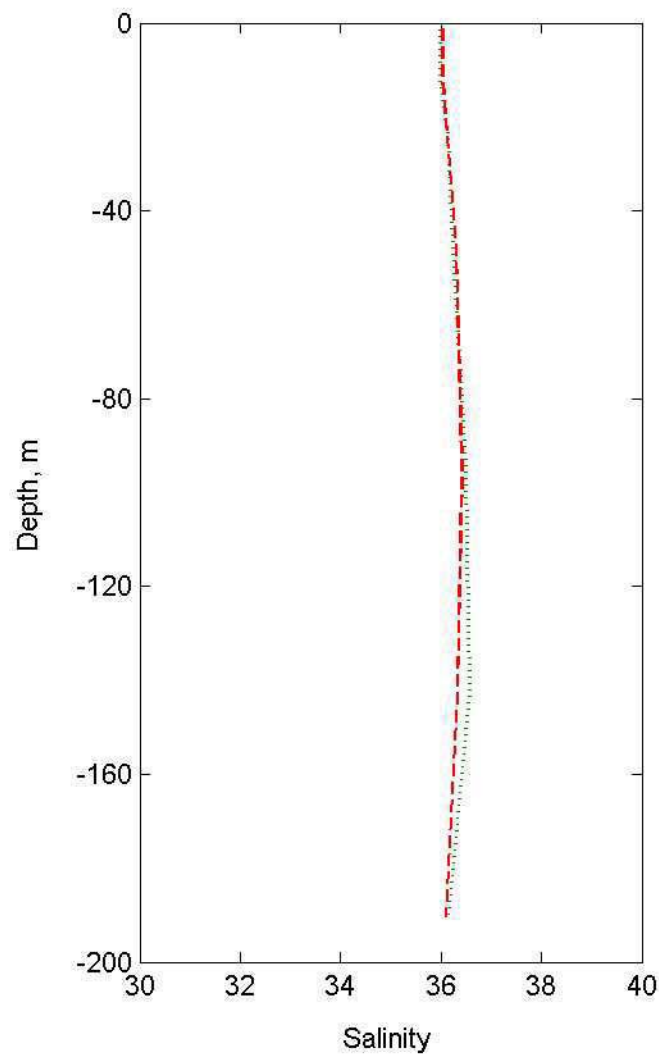
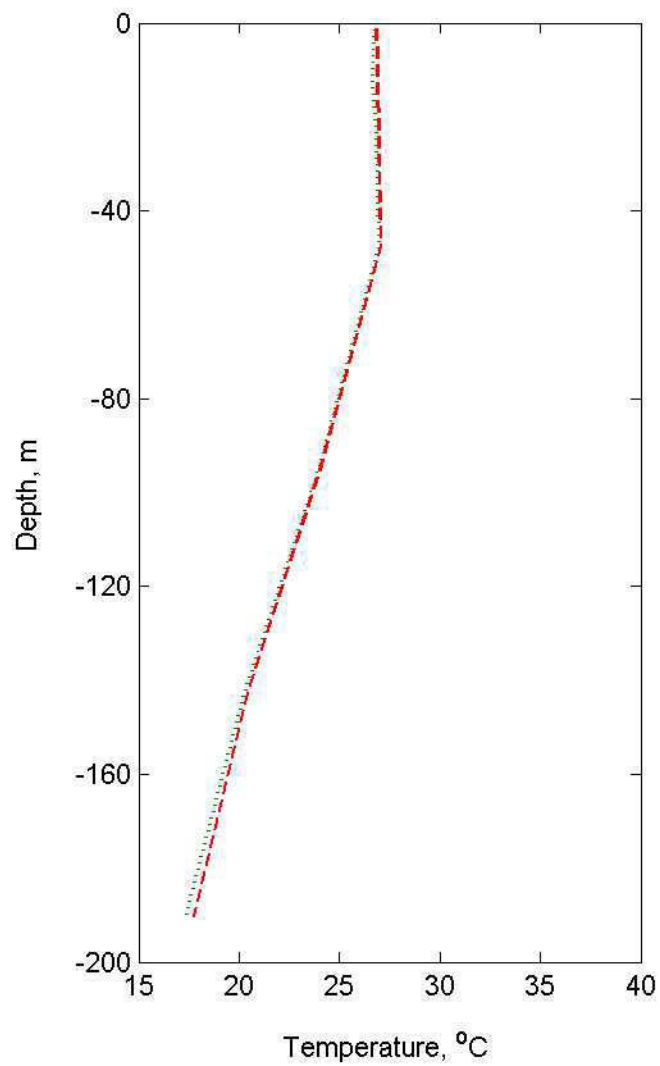


Fig. 6

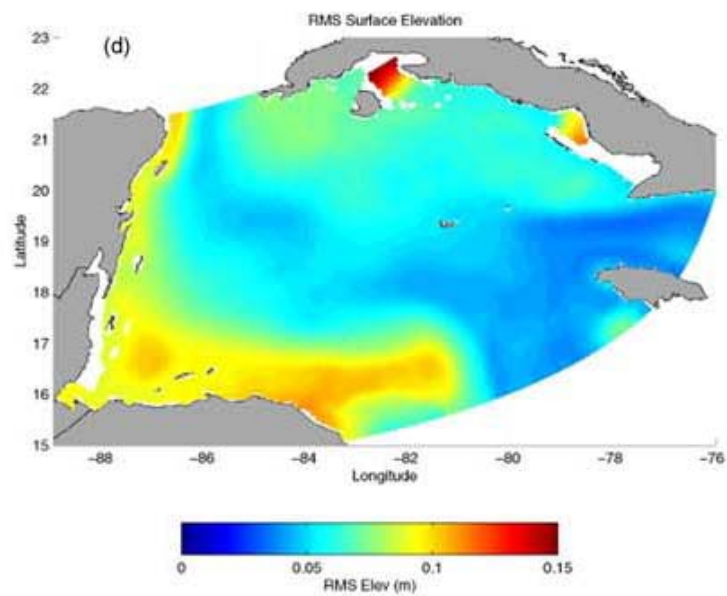
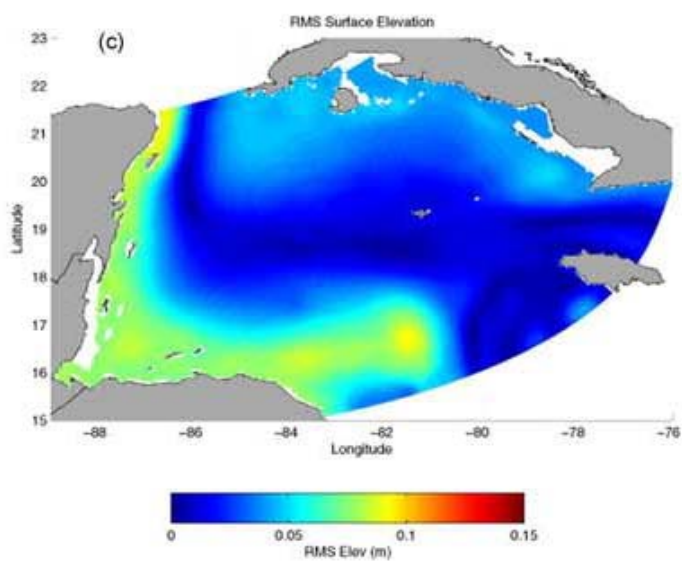
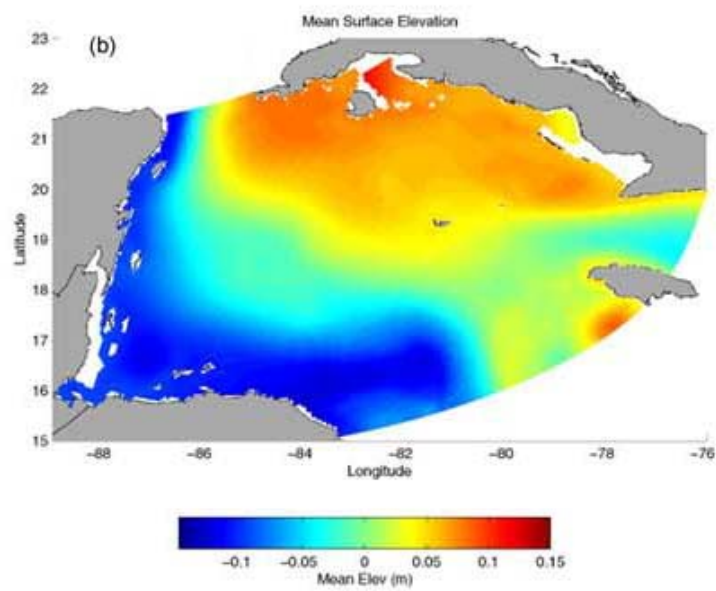
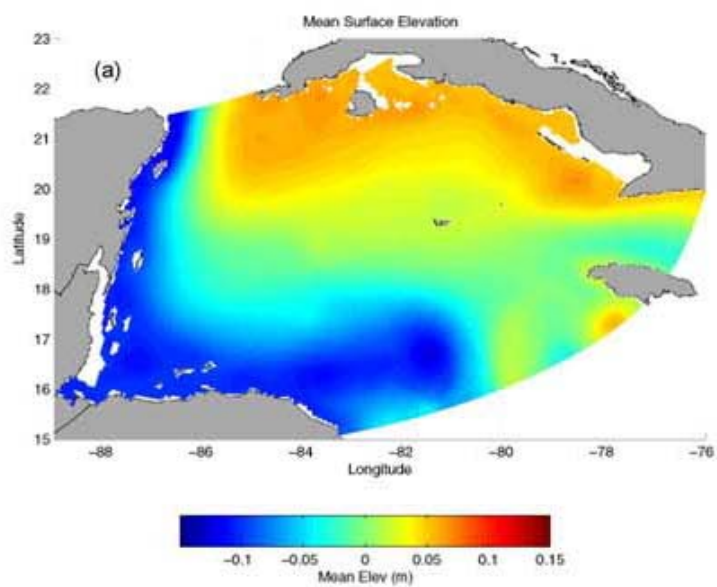
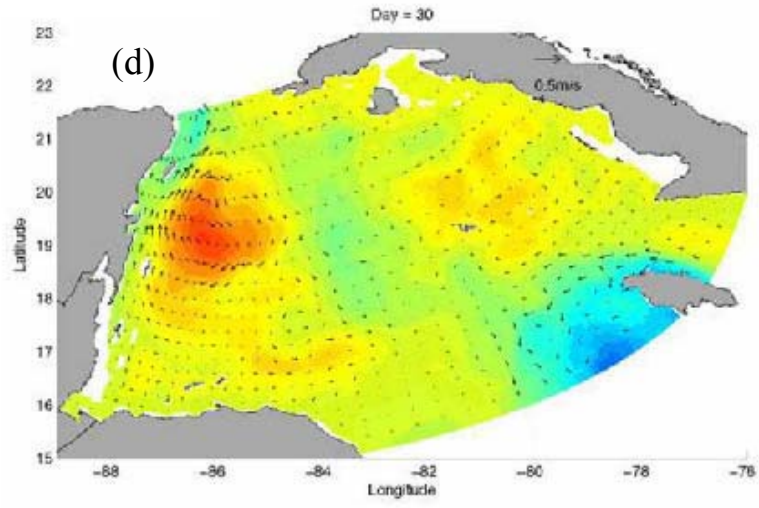
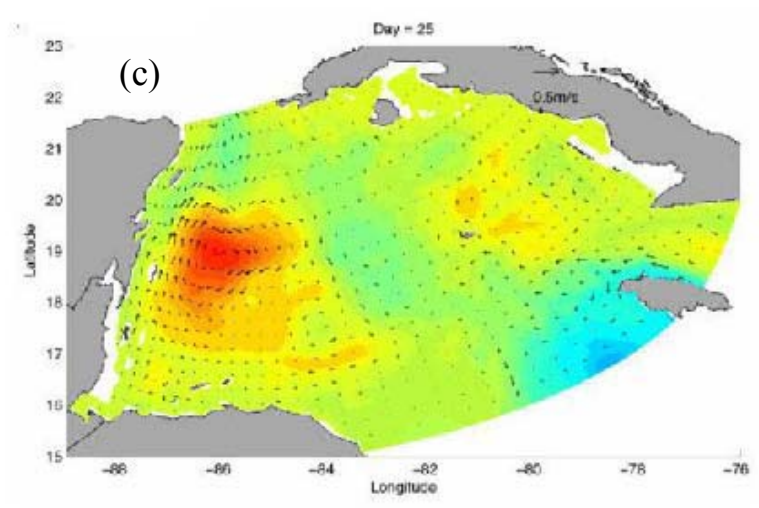
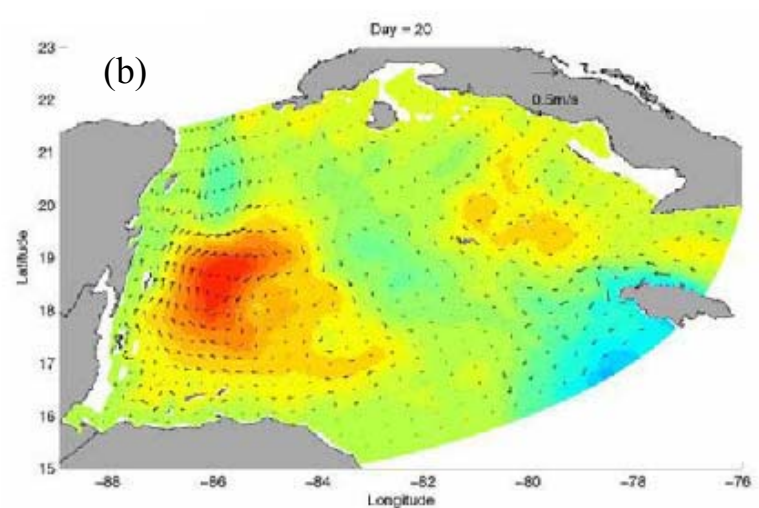
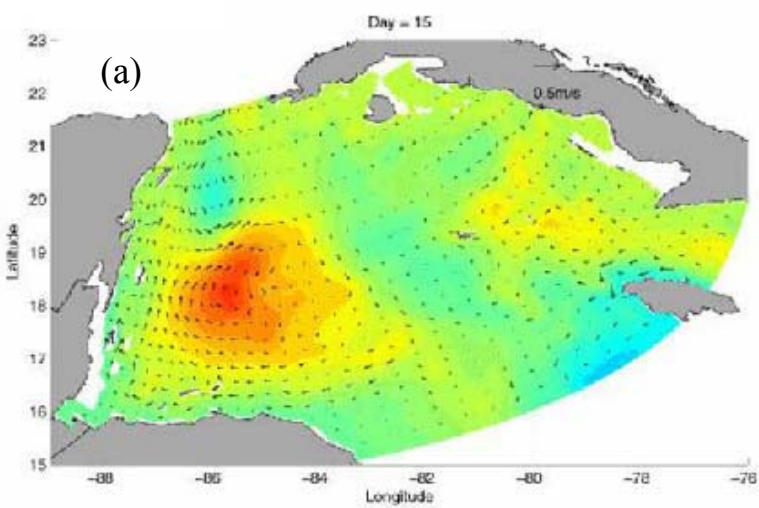
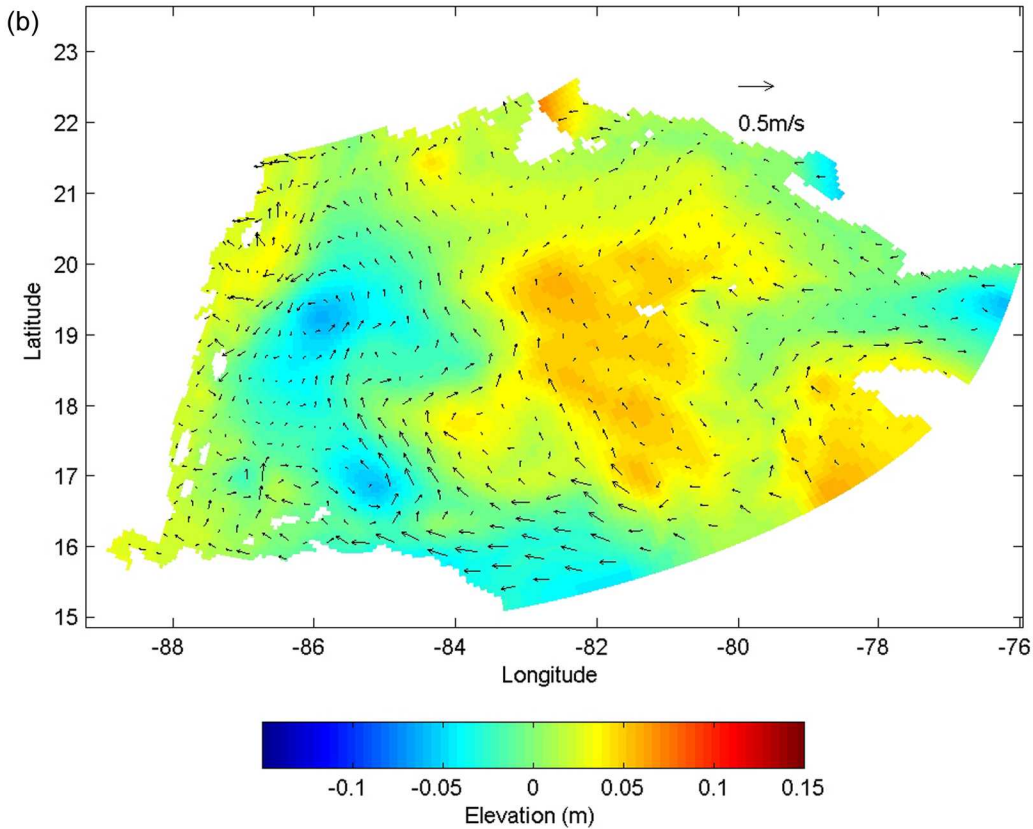
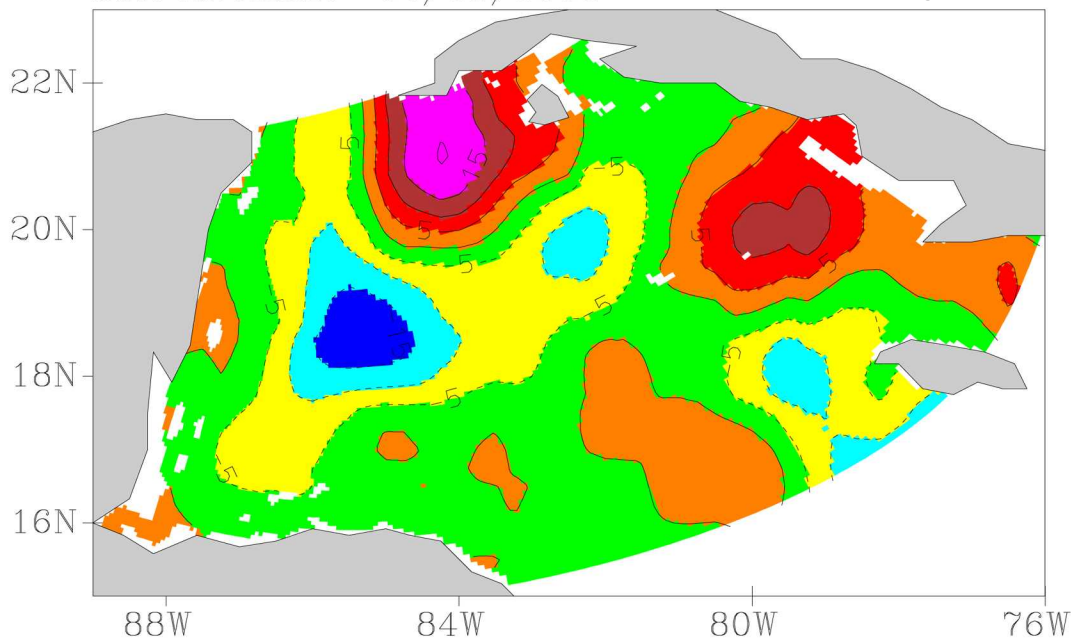


Fig. 7



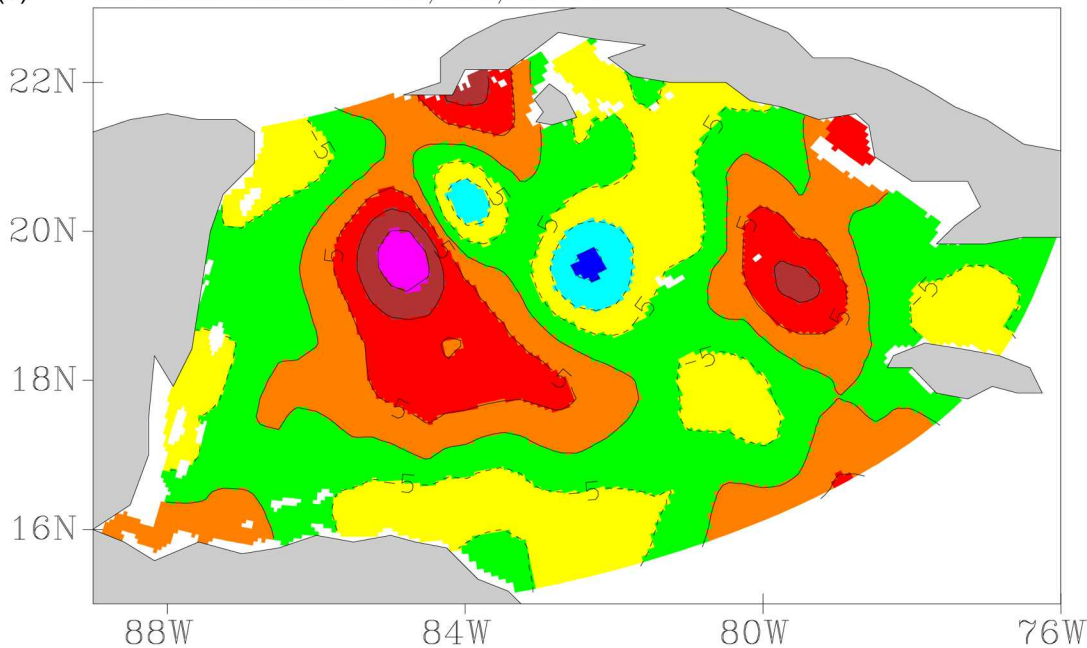
(a) SSH ANOMALY 04/05/1998

Fig. 8



(a) SSH ANOMALY 29/05/1999

Fig. 9



(b)

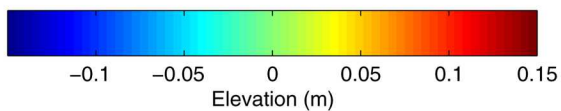
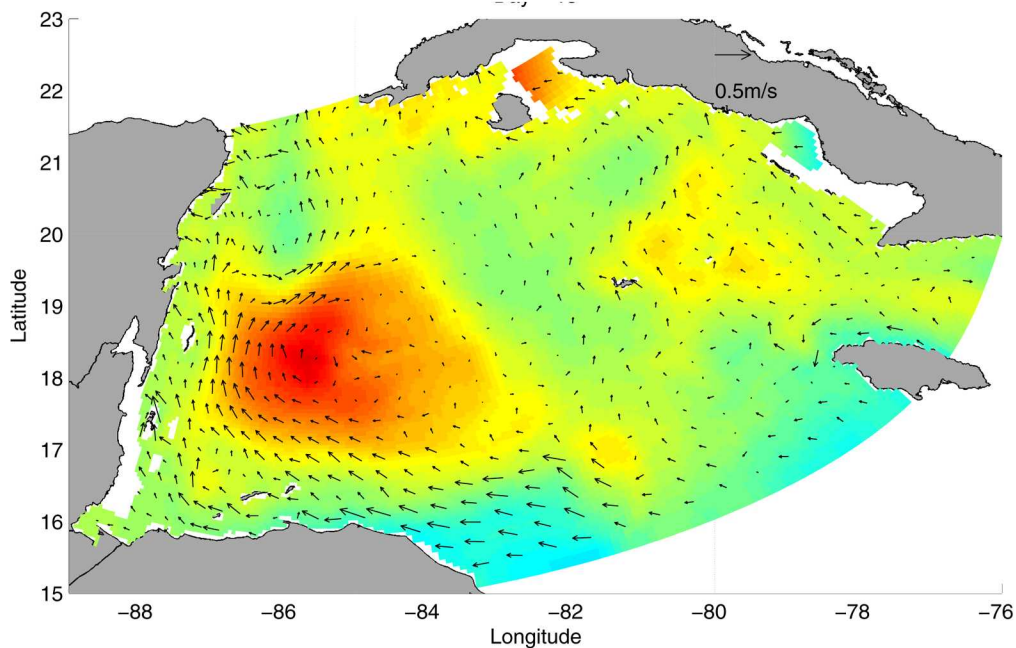


Fig. 10

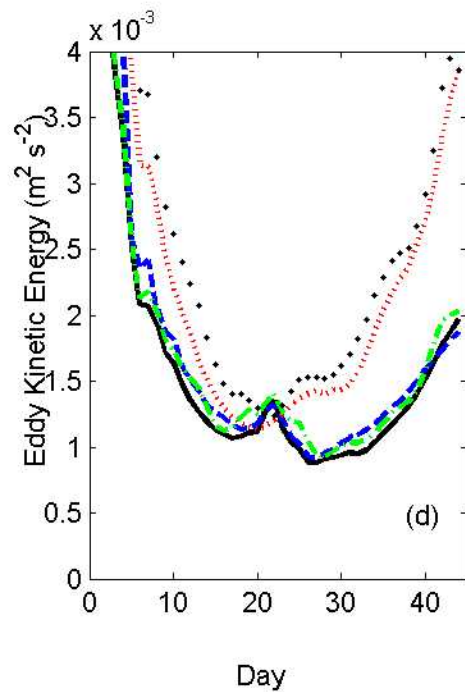
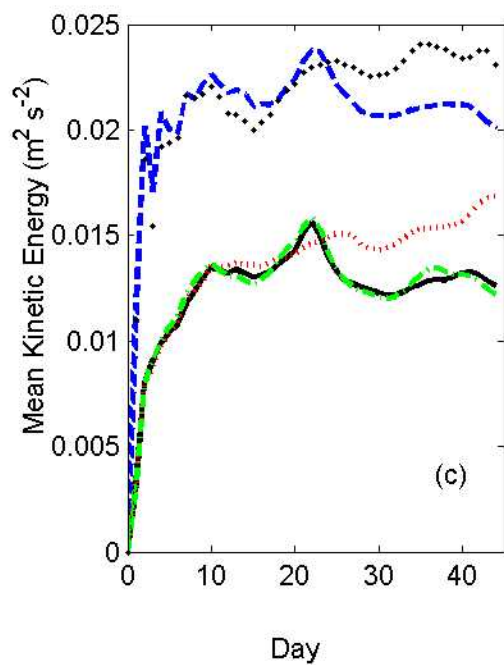
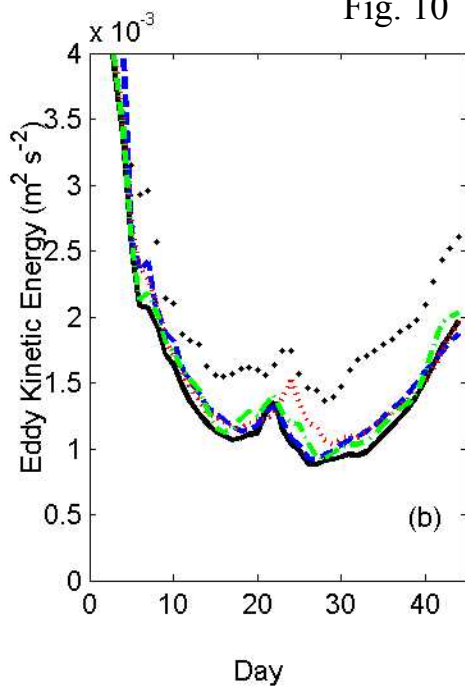
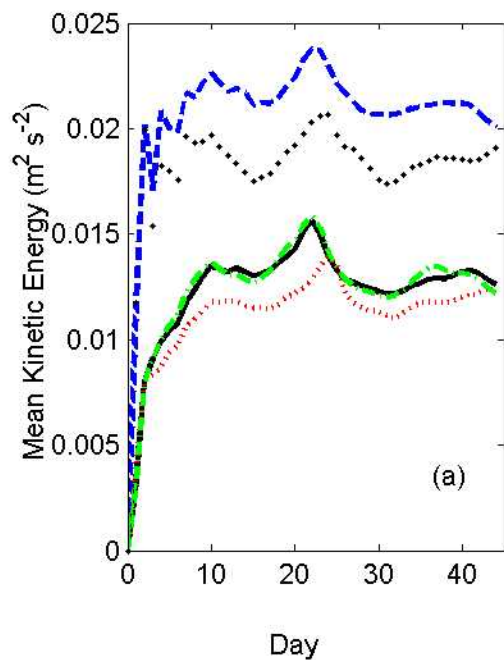


Fig. 11

Lighthouse Reef

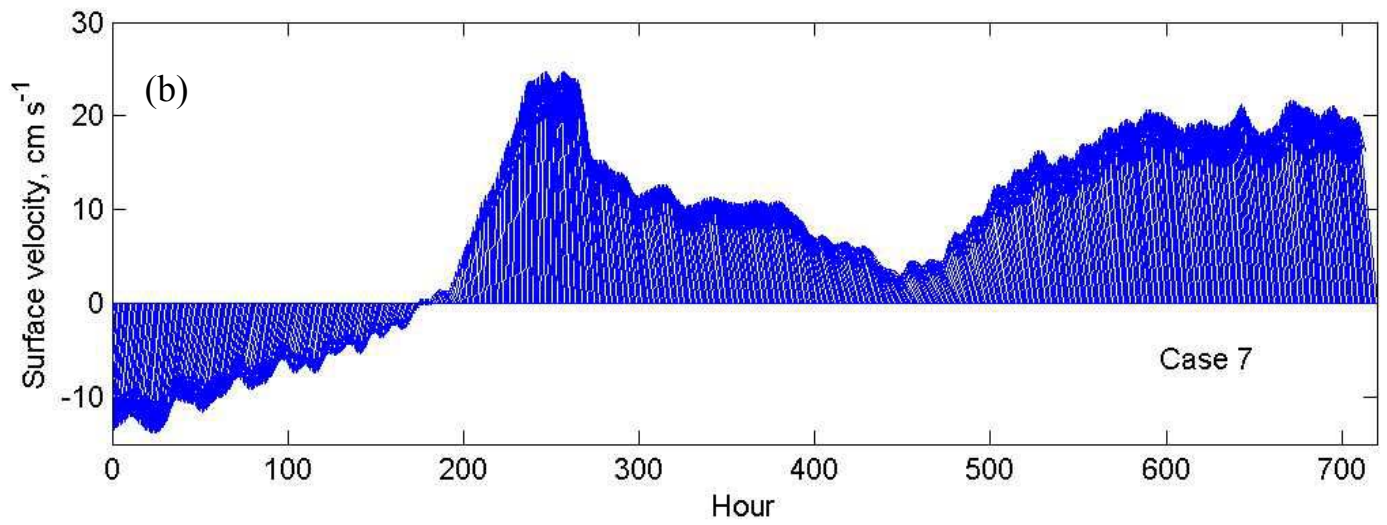
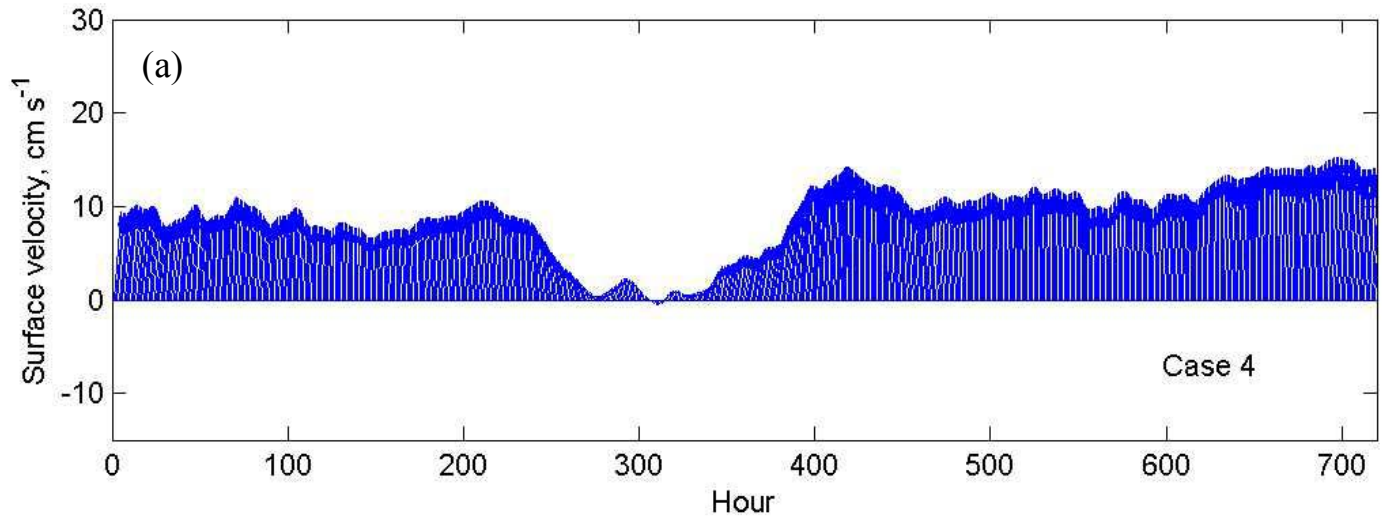


Fig. 12

Gladden Spit

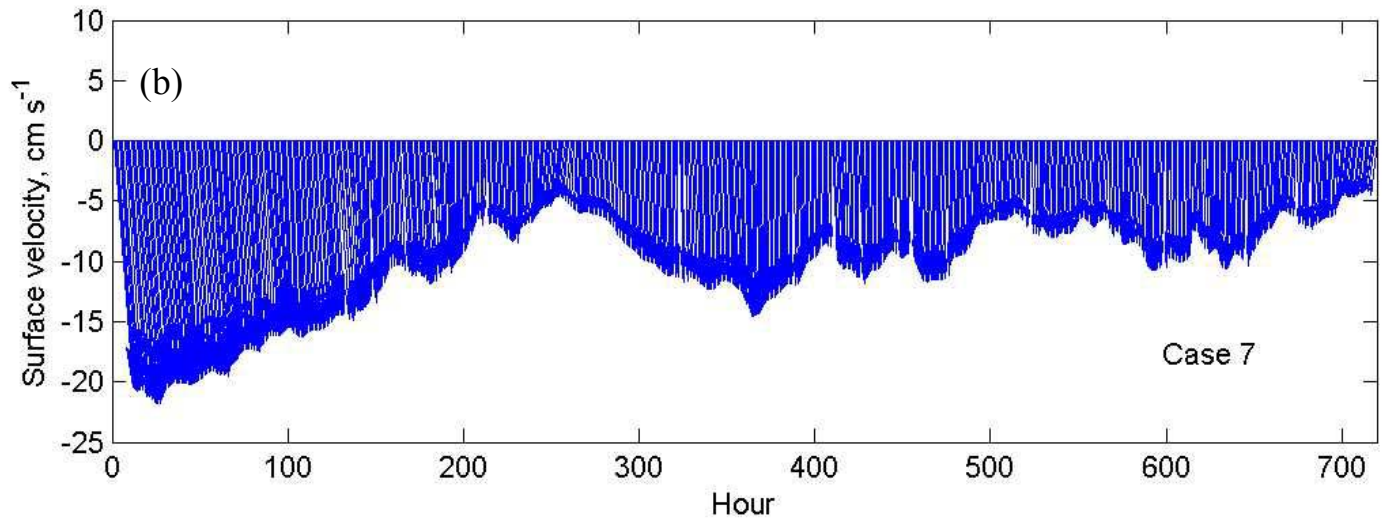
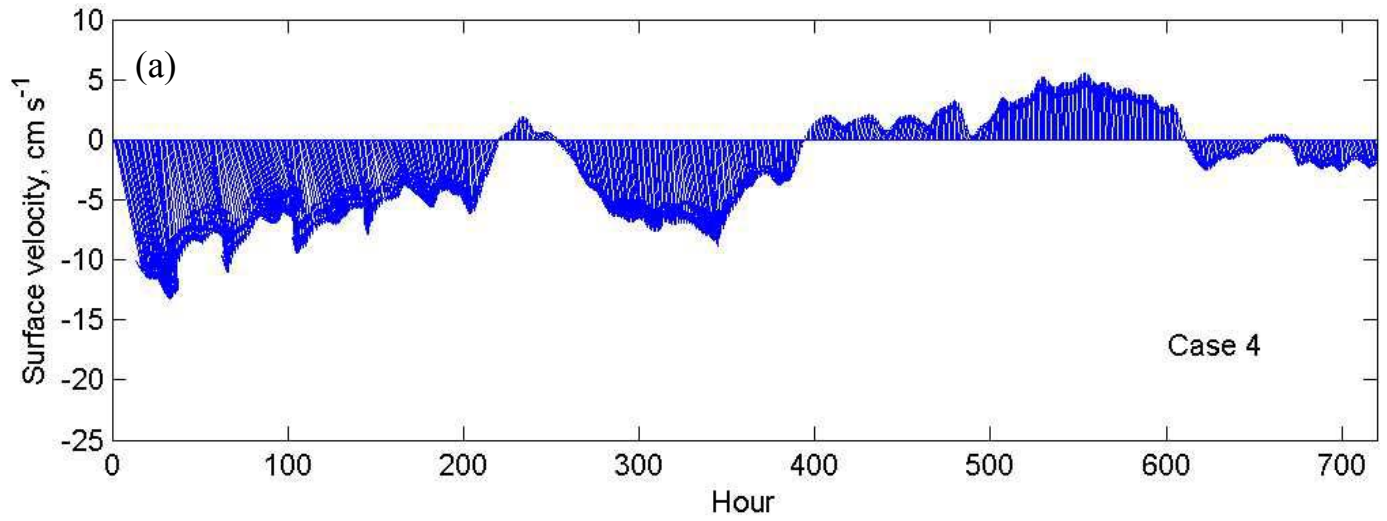


Fig. 13

